

Comparison between electrostatic PP and PIC simulations on electron bunch expansion

Yanan Zhang^{1,2}, Xiaochun Ma², Hui Liu¹, and Yinjian Zhao^{1,*}

¹*School of Energy Science and Engineering, Harbin Institute of Technology, Harbin 150001, People's Republic of China*

²*Harbin Boiler Company Limited, Harbin 150040, People's Republic of China*

^{*}*Corresponding author: Yinjian Zhao, zhaoyinjian@hit.edu.cn*

February 18, 2025

Abstract

With the great development of parallel computing techniques, the particle-particle (PP) model has been successfully applied in a number of plasma applications. Comparing to particle-mesh (PM) models, for example the widely used particle-in-cell (PIC) method, PP has the advantages of high accuracy in solving Coulomb interactions. In this paper, it is shown that PP is also advantageous to simulate non-neutral plasmas, such as electron bunch expansion in vacuum. The numerical effects of the macro-particle weight and the time step length are investigated for a PP model, accurate and convergent results can be obtained with less effort. On the contrary, PIC needs to simulate the same problem with extremely large effort. It is found that the simulation accuracy does not grow with reduced cell size monotonously, thus no convergence can be easily obtained. In the long run, PIC must apply large enough domain to cover all the expanding particles and avoid non-physical effects caused by imperfect infinite boundary condition, which may result in too heavy computation and make PIC infeasible.

1 Introduction

Plasma simulations using particles have been widely applied in numerous areas to solve scientific and engineering problems, such as nuclear fusion [1], particle accelerator [2], plasma propulsion [3], space weather [4], etc. By modeling plasma particles (or macro-particles), the equations of motion are solved along with self-consistent fields and external fields, such that particle trajectories and the relevant physical process can be obtained. In general, plasma simulation methods using particles are more accurate than other approaches, comparing to fluid models for example, because the involved plasma in a particle model can be in non-equilibrium state, and those simulated particles are able to

describe any velocity distribution functions in any transient states, while fluid models are based on the assumption of microscopic equilibrium.

According to the classification of Hockney and Eastwood [5], particle simulation models can be grouped into three broad categories, the particle-particle (PP) model, the particle-mesh (PM) model, and the particle-particle-particle-mesh (PPPM) model. The idea of PP is simple and its implementation is straightforward, i.e., computation of the forces between each pair of particles, but two nested **do** loops usually cannot be avoided, which leads to huge computation ($\propto N_p^2$) as the number of simulated particles N_p increases. Back to the time that the idea of particle simulations was proposed, the computers were way too slow to carry out any meaningful

PP simulations, thus there were rare if not none PP related works on solving plasma problems. Then, the PM model was greatly developed, such as the widely used particle-in-cell (PIC) method [6]. Rather than solving inter-particle forces directly, particles are deposited on mesh points to obtain density values, based on which the fields are solved and interpolated back to particle positions. The PM model can greatly reduce the computation compared to the PP model when many particles are simulated, and the computation scales as $\alpha N_p + \beta(N_c)$, where N_c is the number of cells applied in one dimension, α is a constant, and β is a function depending on the field solver. For example, a typical PIC method solving the electrostatic Poisson's equation would require $\alpha = 20$ and $\beta = 5N_c^3 \log_2 N_c^3$ [5]. However, the increase of computation speed of PM is at the expense of the accuracy, the forces within the range of a cell are neglected, thus the short-range particle interactions can not be resolved. Therefore, the PPPM model was proposed, combining PP to only solve the short-range interactions and PM to reduce the computational cost, which is more often applied in molecular-dynamics simulations [7].

With the great development of parallel computing techniques, the PP model has been picked up in recent years, and a number of successful applications have been carried out for solving different plasma physics problems. For example, because the PP model is good at solving Coulomb collisions with the highest accuracy, it has been applied in high-density collisional plasmas to solve relaxation problems in inertial confinement fusion [8], and it can be used as benchmark to improve Monte Carlo Coulomb collision models [9]. In these applications, no macro-particles are used, namely real electrons and ions are simulated within a small simulation region, such that real Coulomb collisions can be captured by detailed particle trajectories. There are also other areas that do not have that many of charged particles in the considered system, such as in the scenario of plasma propulsion, the plume of electrospray thrusters is made of large charged droplets, where PP is suitable to be applied [10, 11]. By contract, the problem is hard to

be simulated by PIC, because the particles have the same charge, and strong Coulomb forces near the cone jet cause the plume to expand quickly from micrometers to centimeters, thus the mesh resolution of PIC is hard to be coupled in this multi-scale problem.

In this paper, we present another physical problem that is extremely suitable for PP, but very hard for PIC, the electron bunch expansion in vacuum. Such scenario is related to applications of electron pulses for atomic diffraction [12] for example, in which understanding of the electron dynamics of Coulomb spreading is critical [13]. First of all, the system is non-neutral, since only electrons exist, but PIC was originally designed for quasi-neutral plasmas. For example, the cell size criteria is usually determined by the Debye length, which reflects the Debye screening distance only for quasi-neutral plasmas. From the perspective of the PIC algorithm, however, macro-particles of electrons can still deposit their charges on the grid points to obtain the charge density, and the Poisson's equation can still be solved as usual, but it would be difficult for PIC to resolve the forces between particles within a cell. Therefore, there seem to be a trade-off between the accuracy of solving the fields and the computational cost. However, we will show in this paper that using more number of cells may not result in monotonously increasing accuracy, and a convergence could not be achieved. Furthermore, for three dimensional problems, the computational cost is huge for PIC, because the domain size has to be large enough to cover all expanding particles and avoid the non-physical effects caused by imperfect infinite boundary condition. On the contrary, the PP model can simulate an infinite vacuum space straightforwardly, by involving no charges other than the electron bunch.

The numerical effects of the PP model on electron bunch expansion or other similar problems with non-neutral plasmas, have not been studied in detail. Therefore, in this paper, an electron bunch expansion in vacuum is considered, being a representative example of non-neutral plasmas, and the PP and PIC models are both applied and compared to simulate the same problem. Numer-

ical effects of the macro-particle weight and the time step length in PP are studied, and numerical effects of the mesh resolution, the domain size, and the macro-particle shape factor in PIC are investigated. The paper is organized as follows. In Sec.2, the PP algorithm, setup, and simulation results are given. The corresponding PIC simulations are presented in Sec.3. At last, conclusions are drawn in Sec.4.

2 The PP Simulation

2.1 The PP Algorithm and Setup

Initially, an electron bunch is represented by a number of macro-particles N_p . Each macro-particle represents w_p real particles. It is assumed that all macro-particles share the same weight for simplicity. Giving the electron bunch a certain spatial and velocity distribution initially, and putting it in a vacuum, such that the only forces acting on each electron are due to other electrons, the electron bunch will expand over time due to the repulsive Coulomb forces. The Coulomb's law reads

$$\mathbf{F}_{ij} = \frac{1}{4\pi\epsilon_0} \frac{Q_i Q_j}{|\mathbf{r}_{ij}|^2} \hat{\mathbf{r}}_{ij} \quad (1)$$

where \mathbf{F}_{ij} is the Coulomb force acting on the i^{th} macro-particle due to the j^{th} macro-particle, $\mathbf{r}_{ij} = \mathbf{r}_i - \mathbf{r}_j$ is the position vector pointing from the i^{th} macro-particle to the j^{th} macro-particle, $\hat{\mathbf{r}}_{ij} = \mathbf{r}_{ij}/|\mathbf{r}_{ij}|$ denotes the unit vector, Q denotes the charge of the macro-particle and ϵ_0 is the vacuum permittivity. Then, the force acting on the i^{th} macro-particle due to all other macro-particles can be computed through a sum,

$$\mathbf{F}_i = Q_i \mathbf{E}_i = \frac{Q_i}{4\pi\epsilon_0} \sum_{j=1, j \neq i}^{N_p} \frac{Q_j}{|\mathbf{r}_{ij}|^2} \hat{\mathbf{r}}_{ij} \quad (2)$$

where \mathbf{E}_i is the electric field at the position of the i^{th} macro-particle due to all other macro-particles. Eq.(2) can be computed for all macro-particles, then the (non-relativistic) equations of motion can be used to numerically integrate or

update the macro-particle velocities and positions,

$$\frac{d\mathbf{r}_i}{dt} = \mathbf{v}_i \quad (3)$$

$$\frac{d\mathbf{v}_i}{dt} = \frac{\mathbf{F}_i}{M_i} = \frac{Q_i \mathbf{E}_i}{M_i} = \frac{q_i \mathbf{E}_i}{m_i} = \mathbf{a}_i \quad (4)$$

where \mathbf{v}_i denotes the velocity, \mathbf{a}_i denotes the acceleration, M_i denotes the mass of the i^{th} macro-particle, and note that if a real particle has charge q and mass m , the macro-particle charge is $Q = qw_p$ and mass is $M = mw_p$, such that the macro-particle weight can be canceled in Eq.(4). Furthermore, since we are dealing with electrons here with charge $q_e = -e$ and mass m_e , we can simplify Eq.(2), Eq.(3) and Eq.(4) to

$$\mathbf{F}_i = q_e w_p \mathbf{E}_i = \frac{q_e^2 w_p^2}{4\pi\epsilon_0} \sum_{j=1, j \neq i}^{N_p} \frac{\hat{\mathbf{r}}_{ij}}{|\mathbf{r}_{ij}|^2} \quad (5)$$

$$\frac{d^2 \mathbf{r}_i}{dt^2} = \frac{d\mathbf{v}_i}{dt} = \frac{\mathbf{F}_i}{w_p m_e} = \frac{q_e}{m_e} \mathbf{E}_i = \mathbf{a}_i \quad (6)$$

which are the governing equations that close the system for solving the electron bunch expansion.

Because the computation of Eq.(5) for all particles is known to be huge (scale as N_p^2), we apply MPI and OpenMP parallelization right away on the algorithm. The whole particle array containing the positions, velocities, and accelerations of all particles is splitted by different MPI ranks, such that each MPI rank only needs to address its own portion. An additional particle array is used to store the positions of all particles, and the `mpi_allgather` function is used to gather each MPI's particle positions at every time step after the positions are updated. Within each MPI's two nested loops on solving the Coulomb's field, OpenMP is used to further parallelize the code.

Next, we apply the Velocity Verlet method [14] on numerically integrating the equations of motion Eq.(6). The Velocity Verlet method can be summarized as follows. At time step t , we have the position $\mathbf{r}(t)$, the velocity $\mathbf{v}(t)$, and the acceleration $\mathbf{a}(t)$ evaluated based on Coulomb's law using $\mathbf{r}(t)$. Then, we can obtain the new position at time step $t + \Delta t$,

$$\mathbf{r}(t + \Delta t) = \mathbf{r} + \mathbf{v}(t)\Delta t + \mathbf{a}(t)\Delta t^2/2 \quad (7)$$

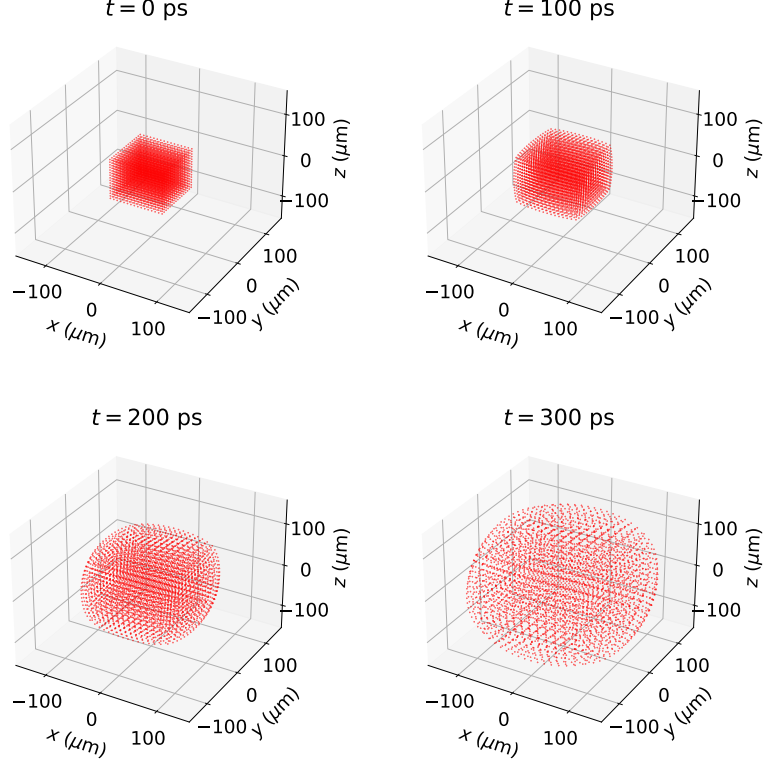


Figure 1: Snapshots at three different times of 3D scatter plots of electron bunch macro-particles.

where Δt denotes the timestep. Next, we can evaluate $\mathbf{a}(t + \Delta t)$ from $\mathbf{r}(t + \Delta t)$ from the Coulomb's law, and obtain the new velocity at $t + \Delta t$,

$$\mathbf{v}(t + \Delta t) = \mathbf{v}(t) + [\mathbf{a}(t) + \mathbf{a}(t + \Delta t)]\Delta t/2 \quad (8)$$

Now, we have obtained $\mathbf{r}(t + \Delta t)$, $\mathbf{v}(t + \Delta t)$, and $\mathbf{a}(t + \Delta t)$, such that the procedure can be repeated to obtain quantities at $t + 2\Delta t$ and so forth.

The simulation initial setup is shown in Fig.1 at 0 time step, where the electron bunch has a cubic shape with exact uniform spatial distribution, i.e., the same inter-particle distances. The reason that a cubic shape is chosen is that it is easier for comparison with the PIC simulation later. The cube size is $l = 0.1$ mm, the electron bunch number density is $n_0 = 5 \times 10^{16} \text{ m}^{-3}$, and the number of macro-particles applied

is $N_p = 16 \times 16 \times 16 = 4096$, which results in a macro-particle weight $w_p = n_0 l^3 / N_p \approx 12.2$. A relatively small timestep is chosen $\Delta t = 10^{-13} \text{ s} = 0.1 \text{ ps}$. For simplicity, the initial velocities of all macro-particles are set to be zero.

2.2 The PP Results

The simulation results are presented in this section. First, snapshots at four different times are shown in Fig.1, which are the macro-particle 3D scatter plots. We can see that due to the Coulomb repulsion, the electron bunch expands overtime. This simulation takes about 532 s to finish 100000 time steps using 64 OpenMP threads and 1 MPI rank on a computer with two AMD EPYC 9174F CPUs.

To verify the validity of the PP results, we first show the influence of the timestep Δt , which is

reduced from 10^{-13} s to 10^{-10} s. The emittance ε_x over time is plotted for four cases with different Δt in Fig.2 (a). Note that the emittance is defined as

$$\varepsilon_x = \sqrt{\langle x^2 \rangle \langle v_x^2 \rangle - \langle x v_x \rangle^2}, \quad (9)$$

which is a statistical quantity to reflect the beam quality in phase space [15], where the angle brackets represent an average over all particles. As we can see, $\Delta t = 10^{-10}$ s is obviously not small enough for the simulation, while the other three smaller Δt leads to closer and more accurate results. As Δt increases 10 times, the total number of time steps needed to finish 10^{-8} s decreases 10 times, thus the simulation can be finished 10 times faster.

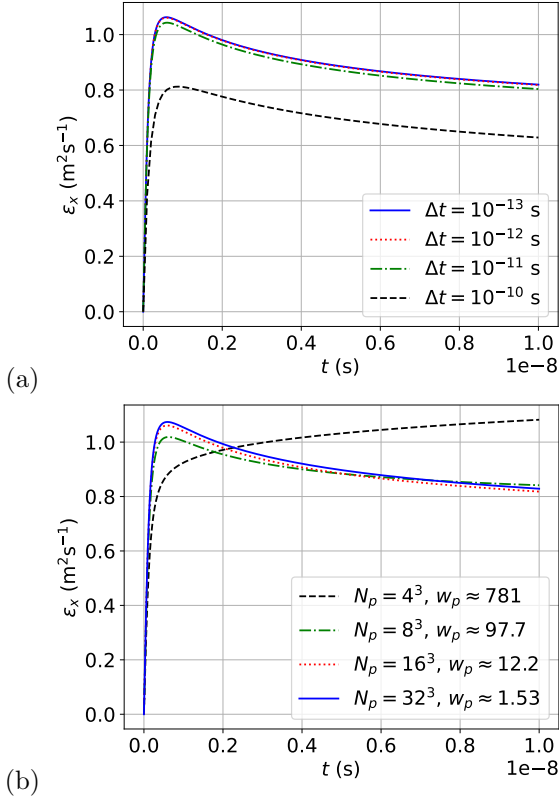


Figure 2: Emittance over time for cases with (a) different timesteps and (b) different number of macro-particles.

Next, we show the influence of the number of

macro-particles N_p (or the macro-particle weight w_p). Four cases are tested from $N_p = 4^3 = 64$ to $N_p = 32^3 = 32768$, while $\Delta t = 10^{-13}$ s is still applied. Note that for the case with $N_p = 32^3$, the macro-particle weight $w_p \approx 1.53$ is already very close to 1, meaning we are pretty much simulating real electrons. The results are shown in Fig.2 (b), we can see that $N_p = 4^3$ is obviously inaccurate, and as N_p increases, the results become more accurate. However, one should note that this physical problem we are dealing with is difficult in terms of long-term accuracy, because the most important physics happens at the very beginning of the simulation, where all electrons are placed within a small region with strong Coulomb forces, any small errors of computing the forces at the beginning will lead to growing errors in macro-particle velocities, positions, and the beam emittance in the long run.

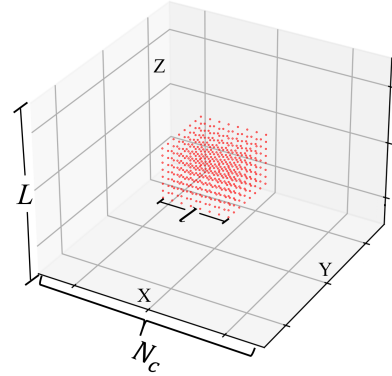


Figure 3: The PIC simulation setup.

3 The PIC Simulation

3.1 The PIC Algorithm and Setup

In this section, we simulate the electron bunch expansion using a standard electrostatic(ES) PIC method, and compare the results to those obtained using the PP model. In an ES PIC, the Poisson's equation is solved based on the charge density on the grid deposited by macro-particles. Note that the electrostatic Poisson's equation is

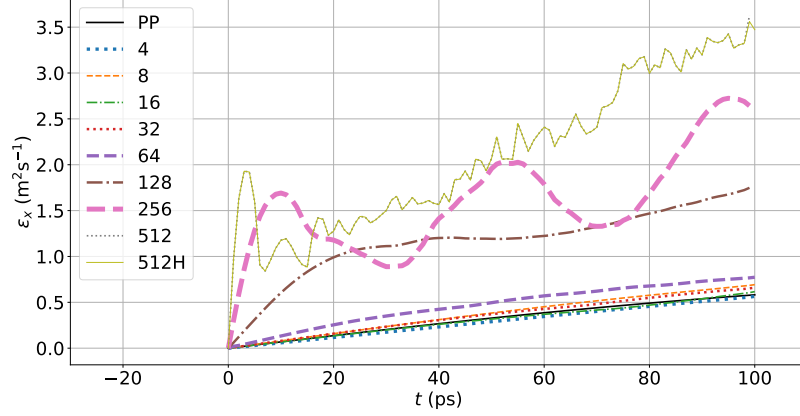


Figure 4: Comparison of emittance between PP and PIC with different mesh resolution. The number of cells per direction N_c is labeled for each curve.

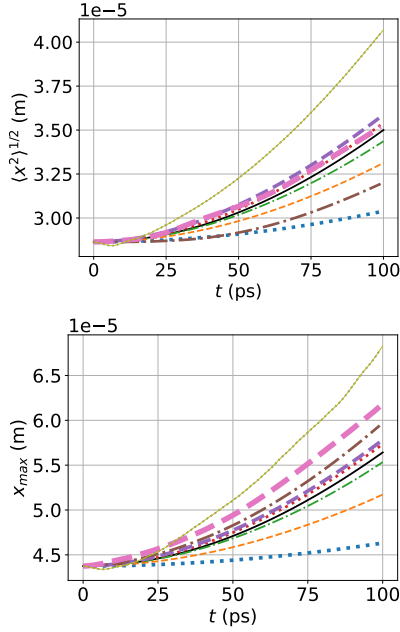


Figure 5: Comparison of $\langle x^2 \rangle^{1/2}$ and x_{max} between PP and PIC with different mesh resolution. The line legend is the same as the one in Fig.4

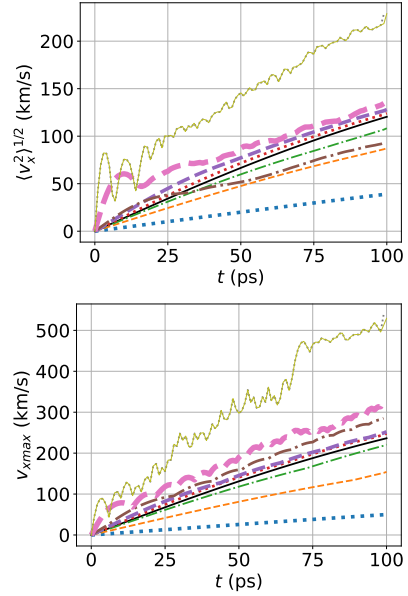


Figure 6: Comparison of $\langle v_x^2 \rangle^{1/2}$ and v_{max} between PP and PIC with different mesh resolution. The line legend is the same as the one in Fig.4

physically equivalent to Coulomb's law, but Poisson's equation is described from the perspective of statistical charge density, while the latter is described by point charges. The PIC code used here

is the open-source PIC code WarpX [16]. WarpX is a highly-parallel and highly-optimized code, which can run on GPUs and multi-core CPUs. WarpX scales to the world's largest supercomputers and was awarded the 2022 ACM Gordon

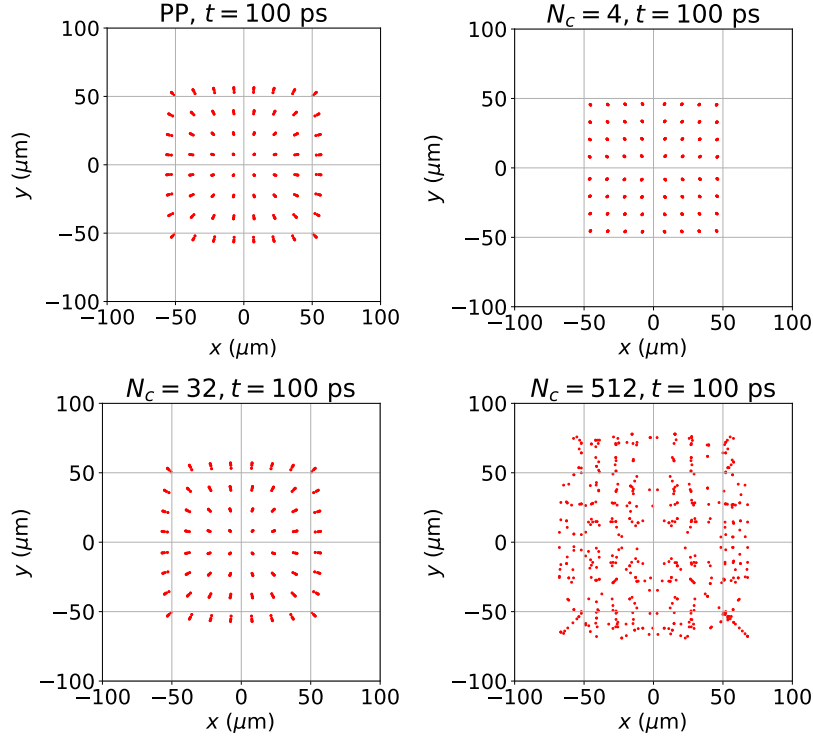


Figure 7: 2D spatial plots of PP and PIC with different mesh resolution.

Bell Prize. The features applied in this paper are the 3D Cartesian geometry, the MLMG (Multi-Level Multi-Grid) electrostatic field solver, the Boris leap-frog particle pusher, and the MPI parallelization.

The PIC simulation domain is set to be a cube with size $L = 0.2$ mm. The macro-particles of the electron bunch are initially placed within a smaller cube with size $l = 0.1$ mm, as illustrated in Fig.3, the same as the preceding PP simulation. The electron bunch number density is still $n_0 = 5 \times 10^{16} \text{ m}^{-3}$ initially. The time step is set to be $\Delta t = 10^{-12}$ s. The number of macro-particles is set to be $N_p = 8^3 = 512$. The WarpX’s MLMG Poisson solver is applied with required precision 10^{-6} (10^{-9} is also tested for one case). The linear density deposition and field interpolation schemes are applied. All faces of the cube are set to be Dirichlet boundary conditions with zero fixed potentials for fields and absorbing boundary conditions for macro-particles.

3.2 The PIC Results and Comparison to PP

Keeping the above parameters fixed, the precision of solving the Poisson’s equation depends on the number of cells per direction N_c , or the cell size L/N_c . Several N_c are tested, ranging from 4 to $2^9 = 512$, namely the cell sizes are varied from $50 \text{ } \mu\text{m}$ to $0.390625 \text{ } \mu\text{m}$. Note that the distance between two macro-particles is $l/8 = 12.5 \text{ } \mu\text{m}$. A corresponding PP test is carried out too, served as an accurate baseline, using the same $N_p = 512$ and $\Delta t = 10^{-12}$ s. The results of emittance ε_x , $\langle x^2 \rangle^{1/2}$, and $\langle v_x^2 \rangle^{1/2}$ are presented in Fig.4, Fig.5, and Fig.6, respectively.

The emittance plot in the Fig.4 shows that the emittances of cases with $N_c \leq 32$ are closer to that of PP, while the emittance of cases with $N_c > 32$ are even worse. This result may be contrary to our first thought that larger N_c with smaller cell size should lead to more accurate and

gradually converged results. However, if we further look at the $\langle x^2 \rangle^{1/2}$ plot in Fig.5(top), we can see that the results of cases $N_c = 256, 64, 32, 16$ are closer to that of PP. The result of $N_c = 128$ is surprisingly worse. In addition, the plot of the maximum value of x among all macro-particles, x_{max} is plotted in Fig.5 (bottom). We can see that this time the lines are in order, an increasing N_c leads to larger x_{max} . Next, look at the $\langle v_x^2 \rangle^{1/2}$ plot in Fig.6 (top), the order is similar to that in Fig.5 (top). The maximum value of v_x among all macro-particles, v_{xmax} , is plotted in Fig.6 (bottom), from which we can see again the lines are in order, an increasing N_c leads to larger V_{xmax} .

The above results indicate that: (1) The accuracy of PIC does not monotonically increase as the cell size decreases. (2) When the cell size is too small, nonphysically large forces appear causing the electron bunch to expand too fast. (3) Because the tendency of the averaged quantities is different from that of the maximum quantities, the locations of macro-particles in the cube or cell matters. The above conclusions can also be confirmed by looking at the 2D spatial plots in Fig.7. When N_c is only 4, the cell size is $50 \mu\text{m}$, bigger than the inter-particle position $12.5 \mu\text{m}$, such that the forces within a cell are weakened, and the electron bunch expands slower. When N_c is 512, the cell size is $0.390625 \mu\text{m}$, so each macro-particle occupies a single cell, and there are about 32 cells between two macro-particles. From the plot, we can see the electron bunch expands faster, and loses its symmetry especially at the diagonals. When N_c is 32, the results are very close to that of PP, and a longer simulation will be conducted later to see if they can match in the long run.

In addition, a higher required precision with 10^{-9} is set for the Poisson solver in PIC for the case $N_c = 512$ labeled as 512H in Fig.4, Fig.5, and Fig.6, since the results overlap with that of the 512 case, the required precision 10^{-6} is sufficient. In terms of the computation speed, the most heavy run with $N_c = 512$ needs to solve the Poisson's equation on a grid system with $512 \times 512 \times 512$ cells for 100 time steps. It takes about 148 s when using 64 MPI with do-

main decomposition $8 \times 8 \times 8$ on a computing node with two AMD EPYC 9754 CPUs. By contract, the corresponding PP run takes only about 0.28 s without parallelization. Thus, under the scenario of the electron bunch expansion, PP is much more accurate and efficient than PIC.

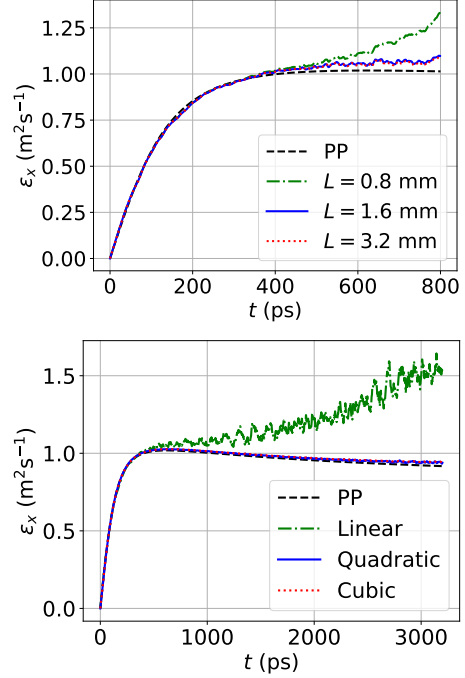


Figure 8: Comparison of emittance between PP and PIC in the long run with varied domain size (top) and varied particle shape-factor (bottom).

3.3 Comparison between PIC and PP in the long run

To further investigate if the $N_c = 32$ case with cell size $6.25 \mu\text{m}$ can match with PP in the long run, three tests are done with fixed cell size, but enlarged N_c and L accordingly to make sure the macro-particles do not move out of the domain and evaluate the effects of the domain size in the meanwhile. $N_c = 128, 256, 512$ are considered and $L = 0.8, 1.6, 3.2 \text{ mm}$ are varied accordingly. The results of the emittance growth until 800 ps are plotted in Fig.8 (top). As we can see, all three

cases match well with PP at the beginning until about 400 ps. Then the $L = 0.8$ mm case deviates the most from PP, indicating the domain size is not large enough, since a fixed potential Dirichlet boundary condition is used, which is not a perfect infinite boundary. The cases with $L = 1.6$ and 3.2 mm overlap with each other, indicating that further enlarging the domain size cannot contribute to obtain more accurate results, which would be due to the fact that after the electron bunch expands, eventually each macro-particle occupies a single cell, and there are more and more cells between two adjacent macro-particles, so the fields cannot be solved accurately anymore, just as shown already by the $N_c = 512$ case in Fig.4, Fig.5, Fig.6, and Fig.7.

At last, another even longer run till 3200 ps is carried out varying the particle shape factor from linear, quadratic, to cubic. To let the PIC simulation domain still contains all particles till 3200 ps, while maintaining the cell size unchanged, $N_c = 1024$ and $L = 6.4$ mm have to be set, resulting in a simulation time of about 37 hours using 64 MPI ranks. However, the corresponding PP run only takes 23 s without parallelization. The emittance results are shown in Fig.8 (bottom). As we can see, the linear case deviates from PP obviously after about 800 ps, while the quadratic and cubic shape factors lead to only small deviation at 3200 ps. Thus higher-accuracy shape factors contribute for PIC to obtain better results in electron bunch expansion.

4 Conclusion

In this paper, under the scenario of electron bunch expansion in vacuum due to Coulomb repulsion, the PP model and the PIC model are compared in detail. For the PP model applied, there are only two factors that determine the accuracy, one is the macro-particle weight, the other is the time step length. Simulation results indicate that decreasing the macro-particle weight and the time step length leads to converged results, and little effort is needed for the PP model to conduct accurate simulations of electron bunch expansion. On the contrary, it

is very hard for PIC to simulate electron bunch expansion, because the domain size needs to be large enough to contain all expanding particles, and the mesh resolution cannot be too coarse and needs to be chosen carefully. It is found that the relation between the mesh resolution and the simulation accuracy is not monotonous, thus no convergence can be obtained. When the cell size is close to the initial inter-particle distance, fairly accurate simulation results can be obtained. The precision of the Poisson solver has minor effects on the simulation, and 10^{-6} seems to be small enough. In the long run, as the electron bunch expands more and occupies a bigger region, PIC must use a large enough domain to cover all the particles and avoid non-physical effects caused by imperfect infinite boundary condition, so the computation becomes too expensive and unfeasible. In addition, it is found that the particle shape factors matter, quadratic and cubic shape factors lead to more accurate results than linear in the long run.

Acknowledgment

The authors acknowledge the support from National Natural Science Foundation of China (Grant No. 5247120164). This research used the open-source particle-in-cell code WarpX <https://github.com/ECP-WarpX/WarpX>, primarily funded by the US DOE Exascale Computing Project. Primary WarpX contributors are with LBNL, LLNL, CEA-LIDYL, SLAC, DESY, CERN, and TAE Technologies. We acknowledge all WarpX contributors.

Data Availability

The data that support the findings of this study are available from the corresponding author upon reasonable request.

5 References

- [1] Drew Pitney Higginson, Anthony Link, and Andrea Schmidt. A pairwise nuclear fu-

- sion algorithm for weighted particle-in-cell plasma simulations. *Journal of Computational Physics*, 388:439–453, 2019. doi:[10.1016/j.jcp.2019.03.020](https://doi.org/10.1016/j.jcp.2019.03.020).
- [2] Y. Zhao, R. Lehe, A. Myers, M. Thévenet, A. Huebl, C. B. Schroeder, and J.-L. Vay. Plasma electron contribution to beam emittance growth from coulomb collisions in plasma-based accelerators. *Physics of Plasmas*, 29(10):103109, 10 2022. doi:[10.1063/5.0102919](https://doi.org/10.1063/5.0102919).
- [3] Baisheng Wang, Tianhang Meng, Yinjian Zhao, Zhongxi Ning, Hui Liu, and Daren Yu. Electromagnetic particle-in-cell simulation on self-induced magnetic field by hollow cathode discharge. *Plasma Sources Science and Technology*, 32(9):095009, sep 2023. doi:[10.1088/1361-6595/acf7e7](https://doi.org/10.1088/1361-6595/acf7e7).
- [4] S. Peter Gary, Yinjian Zhao, R. Scott Hughes, Joseph Wang, and Tulasi N. Parashar. Species entropies in the kinetic range of collisionless plasma turbulence: Particle-in-cell simulations. *The Astrophysical Journal*, 859(2):110, may 2018. doi:[10.3847/1538-4357/aac022](https://doi.org/10.3847/1538-4357/aac022).
- [5] R. W. Hockney and J. W. Eastwood. *Computer Simulation Using Particles*. Adam Hilger, 1988.
- [6] C.K. Birdsall and A.B. Langdon. *Plasma Physics via Computer Simulation*. Bristol: Adam Hilger, 1991.
- [7] Guy Dimonte and Jerome Daligault. Molecular-dynamics simulations of electron-ion temperature relaxation in a classical coulomb plasma. *Phys. Rev. Lett.*, 101:135001, Sep 2008. doi:[10.1103/PhysRevLett.101.135001](https://doi.org/10.1103/PhysRevLett.101.135001).
- [8] Yinjian Zhao. Investigation of effective impact parameters in electron-ion temperature relaxation via particle-particle coulombic molecular dynamics. *Physics Letters A*, 381(35):2944–2948, 2017. doi:[10.1016/j.physleta.2017.05.066](https://doi.org/10.1016/j.physleta.2017.05.066).
- [9] Yinjian Zhao. A binary collision monte carlo model for electron-ion temperature relaxation. *Physics of Plasmas*, 25(3):032707, 03 2018. doi:[10.1063/1.5025581](https://doi.org/10.1063/1.5025581).
- [10] Yinjian Zhao and Joseph Wang. A particle-particle simulation model for droplet acceleration in colloid thrusters. In *the 36th International Electric Propulsion Conference*, pages IEPC–2019–526, 2019.
- [11] McKenna J.D. Breddan and Richard E. Wirz. Electrospray plume evolution: Influence of drag. *Journal of Aerosol Science*, 167:106079, 2023. URL: <https://www.sciencedirect.com/science/article/pii/S002185022200115X>, doi:[10.1016/j.jaerosci.2022.106079](https://doi.org/10.1016/j.jaerosci.2022.106079).
- [12] A. Gliserin, M. Walbran, F. Krausz, and P. Baum. Sub-phonon-period compression of electron pulses for atomic diffraction. *Nature Communications*, 6:8723, 2015. doi:[10.1038/ncomms9723](https://doi.org/10.1038/ncomms9723).
- [13] I. V. Kochikov, R. J. Dwayne Miller, and A. A. Ischenko. Relativistic modeling of ultra-short electron pulse propagation. *Journal of Experimental and Theoretical Physics*, 128:333–340, 2019. doi:[10.1134/S1063776119020201](https://doi.org/10.1134/S1063776119020201).
- [14] William C. Swope, Hans C. Andersen, Peter H. Berens, and Kent R. Wilson. A computer simulation method for the calculation of equilibrium constants for the formation of physical clusters of molecules: Application to small water clusters. *The Journal of Chemical Physics*, 76(1):637–649, 01 1982. arXiv:https://pubs.aip.org/aip/jcp/article-pdf/76/1/637/18934474/637%5B1%5D_online.pdf, doi:[10.1063/1.442716](https://doi.org/10.1063/1.442716).
- [15] Klaus Floettmann. Some basic features of the beam emittance. *Phys. Rev. ST Accel. Beams*, 6:034202, Mar 2003. URL: <https://link.aps.org/doi/10.1103/PhysRevSTAB.6.034202>, doi:[10.1103/PhysRevSTAB.6.034202](https://doi.org/10.1103/PhysRevSTAB.6.034202).

- [16] Luca Fedeli, Axel Huebl, France Boillod-Cerneux, Thomas Clark, Kevin Gott, Conrad Hillairet, Stephan Jaure, Adrien Leblanc, Rémi Lehe, Andrew Myers, Christelle Piechurski, Mitsuhsa Sato, Neïl Zaim, Weiqun Zhang, Jean-Luc Vay, and Henri Vincenti. Pushing the frontier in the design of laser-based electron accelerators with groundbreaking mesh-refined particle-in-cell simulations on exascale-class supercomputers. In *SC22: International Conference for High Performance Computing, Networking, Storage and Analysis*, pages 1–12, 2022. [doi:10.1109/SC41404.2022.00008](https://doi.org/10.1109/SC41404.2022.00008).